Dielectric Constant and Structure of Liquid 18-Crown-6 Calculated from Molecular Dynamics Simulations

F. T. H. Leuwerink* and W. J. Briels

Chemical Physics Laboratory, University of Twente, P.O. Box 217, 7500 AE Enschede, The Netherlands

Received: May 14, 1996; In Final Form: September 6, 1996[⊗]

The results are presented for molecular dynamics simulations of liquid 18-crown-6 using different potential models. The results offer the possibility of investigating the influence of the flexibility of the dihedral angles and the effects of the united atom approach. The radial distribution functions and the correlation between the molecular separations and relative orientations are found to be rather insensitive to the specific potential model used. The relation between orientation correlations and dipole−dipole correlations on the other hand is found to be very sensitive to the flexibility of the molecule. The contributions of the dipole−dipole correlations to the dielectric constant are found to be small compared to those of the molecular dipoles. The calculated dielectric constants are very much in disagreement with the experimental one. It is believed that adding electronic polarization terms to the potential models will very much enhance the contributions of the dipole−dipole correlations to the dielectric constant without necessarily changing the molecular and structural properties.

1. Introduction

Approximately 15 years ago, the importance of the correct treatment of long-range forces in computer simulations in order to obtain reliable dielectric properties, was recognized.[1−3] These long-range electrostatic interactions are usually treated in one of two ways. In the reaction field method[4−6] the interactions are truncated at some cutoff distance r_c. The interactions beyond r_c are approximated as being due to an infinite continuum of a given permittivity. In this case, if a truly infinite system is to be modeled, the permittivity of the continuum should correspond to that of the system being simulated; otherwise, a small discontinuity will exist at r_c. In the alternative method, the Ewald summation method,[7,8] which is a technique for efficiently summing the interactions between an ion or molecule with all its periodic images, there is essentially no truncation of the electrostatic interactions.

In the early 1980s Neumann and Steinhauser published a number of papers[9−15] in which they clarified the relation between the dielectric properties and the different types of boundary conditions that can be employed in simulations. Since then, many papers have appeared on this subject. Most of them were concerned with the properties of simple atomic liquids like the Stockmayer point dipole[16] and hard-sphere and soft-sphere point dipole liquids.[17,18] Besides these simple atomic liquids, a great deal of effort has been put into the study of several potential models for water.[19−24] As a widely used solvent in simulations the question of the dielectric response is especially important in calculations in which the electrostatic interactions predominate, for instance ionic solutions and biochemical systems. Recently, the static and frequency-dependent dielectric properties of two complex protein molecules were calculated.[25]

In this article we calculate the dielectric response of the moderately complex organic liquid 18-crown-6. The 18-crown-6 molecule has been the subject of numerous molecular dynamics and mechanics studies. In many of these investigations a great deal of attention was given to conformational statistics, whereas some of these studies even focused entirely on the calculation of statistical properties.[26−37] For this, the crown ether molecule was either simulated *in vacuo* or in solution. Much of the data obtained from these simulations cannot easily be compared with experiment.

Among the calculations mentioned above there is hardly any consistency as far as the force field parameters for the crown ether molecule are concerned. Different sets of parameters were used, and sometimes parameters originating from different sources were combined. As a result, at present many different force fields exist for the calculations of the properties of 18-crown-6 (see ref 38). It is probably fair to say that the large number of different potential models reflects the restricted applicability of most of them.

When putting the various force fields to a test, it turns out that many properties do not seem to be very sensitive to the applied force field. For instance, with different force fields the structure adopted in the crystal, which is of C_i symmetry, was indeed the lowest energy conformation. van Eerden *et al.*,[40] who calculated from simulations of crystalline 18-crown-6 the thermal shortening of covalent bonds observed in X-ray diffraction experiments, found that this shortening is rather insensitive to the force field that is used.

In a second group of papers, complexation properties were studied by means of free energy calculations.[41,43−45] And although different potential models were used in these investigations, most of the calculated free energy differences compare quite well with experiment. In these cases solvation effects dominate the complexation processes, and so the model used for the solvent may conceal possible flaws of the force field employed for the crown ether.

Recently, we investigated the dipole moment of 18-crown-6 using different sets of charges for the crown.[38] With charges taken from a recently published paper[39] (potential A), the experimental dipole moment was well reproduced. A second potential (potential B) was used by Kowall and Geiger[46] in a study of the association of 18-crown-6 with potassium in aqueous solution, finding an activation barrier for this process in good agreement with experiments. A third potential (potential C) differs from the one used by Kowall and Geiger in the torsional pararmeters. This offers the possibility to not only

[⊗] Abstract published in *Advance ACS Abstracts,* January 1, 1997.

S1089-5647(96)01390-9 CCC: $14.00

look for the best potential possible but also study the influence of flexibility on the properties of the liquid.

In this paper we use the three force fields mentioned above to calculate the dielectric constant of liquid 18-crown-6 (section 4.1). In section 4.2, we study the structure of the liquid. In the next section the methods and procedures of the simulations are described, and in section 3 an overview is given of the potential models that are used in the present calculations.

2. Methods

When using the Ewald summation, which is the method we employed for calculating the electrostatic interactions, the central simulation box is considered to be embedded in an infinite lattice of identical boxes, and the electrostatic energy of the central box is calculated by summing the interactions of all molecules in the central box with their complete surroundings. The essence of the Ewald method is the fact that the conditionally convergent sum over the Coulomb interactions is transformed into two absolutely convergent sums, one in real space and the other in reciprocal k space.[8]

When the system is considered to consist of (partially) charged atoms, the electrostatic energy reads:[47,48]

$$V = \frac{1}{2L}\sum_i\sum_j \left[q_i q_j \sum_{\mathbf{n}} \frac{\mathrm{erfc}(\alpha|\mathbf{r}_{ij}^{\mathrm{norm}} + \mathbf{n}|)}{|\mathbf{r}_{ij}^{\mathrm{norm}} + \mathbf{n}|} + \sum_{\mathbf{k}\neq 0} \frac{1}{\pi k^2} \exp\left(-\frac{\pi^2 k^2}{\alpha^2}\right) \cos(2\pi \mathbf{k}\cdot\mathbf{r}_{ij}^{\mathrm{norm}}) \right] - \frac{2\pi}{(2\epsilon_s + 1)L} \left(\sum_i q_i r_i^{\mathrm{norm}}\right)^2 - \frac{1}{L}\frac{\alpha}{\pi^{1/2}} \sum_i q_i^2 \quad (1)$$

Here, erfc(x) is the complementary error function. q_i is the charge on atom i and $\mathbf{r}_{ij}^{\mathrm{norm}} = \mathbf{r}_{ij}/L$, $\mathbf{r}_{ij}$ being the position vector of atom i relative to atom j and L the length of the computational box. $\mathbf{n}$ and $\mathbf{k}$ run through all triples (n_1, n_2, n_3) of integers n_i; when $\mathbf{n} = (0,0,0)$, terms with $i = j$ should be excluded in the real space sum. α is a convergence parameter which controls the relative weights of the real space and the reciprocal space sums. If α is chosen to be large enough, the only terms which contribute to the sum in real space are those corresponding to the nearest image convention. The term in eq 1 containing ϵ_s is the so-called surface term and depends on the dielectric that surrounds the Ewald sphere. Like is often done, we chose the Ewald sphere to be surrounded by a good conductor, i.e., $\epsilon_s = \infty$, so this term vanishes. The last term in eq 1 is the self-energy term and subtracts the contributions of charges interacting with themselves, which are contained in the real space sum.

Because the above sum also includes unwanted interactions of charges within one molecule, an extra term

$$V^{\mathrm{intra}} = \frac{1}{2}\sum_m \sum_{a=1}^{n_s} q_{ma} \sum_{b\neq a} \frac{q_{mb}}{d_{ab}} \quad (2)$$

has to be subtracted. Here m runs through all molecules in the central box, n_s is the number of atoms per molecule, and d_{ab} is the intramolecular separation of atoms a and b. The sum over b is restricted to the nearest and second-nearest neighbors of atom a.

From a simulation the relative permittivity, ϵ, of the system can be obtained via the fluctuations of the total dipole moment of the system. In SI units the relation is given by[10]

$$\frac{\epsilon - 1}{\epsilon + 2} = \frac{(\langle \mathbf{M}^2\rangle - \langle \mathbf{M}\rangle^2)}{9\epsilon_0 V kT}\left(1 - \frac{\epsilon - 1}{\epsilon + 2}Q\right) \quad (3)$$

where Q is related to the integral of the dipole−dipole tensor and is a function of the Ewald parameter:

$$Q = \int 4\pi r^2 \, \mathrm{d}r \left(\frac{\alpha}{\pi^{1/2} L}\right)^3 \exp\left(\frac{-\alpha^2 r^2}{L^2}\right) \quad (4)$$

In the minimum image convention the integral would extend over the whole basic simulation cell. Here, however, we used a further truncation whereby only particles inside a specific cutoff radius, r_c, are considered. The integral of eq 4 is therefore over a sphere with radius r_c.[10]

In an ideal simulation the potential is not truncated, and in the Ewald sum of eq 1 all images of the central simulation cell in the real space sum and all $\mathbf{k}$ vectors in the k space sum are included. In this ideal case $Q = 1$. Calling $\tilde{\epsilon}$ the permittivity obtained with eq 3 when Q is put equal to one, one can easily show that

$$\epsilon = \frac{(Q + 2)(\tilde{\epsilon} - 1) + 3}{(Q - 1)(\tilde{\epsilon} - 1) + 3} \quad (5)$$

Kusalik has shown that the above correction for the reduced accuracy can be an overestimate when the system does not behave like a macroscopic dielectric.[49]

In the molecular dynamics simulations reported here we modeled a cubic box containing 125 18-crown-6 molecules. The initial boxes were prepared with all molecules in the D_{3d} conformation. First, the energy of the box was minimized. Because the sampled section of the crown's vast conformation space is correlated with the starting conformation of the molecule, the system was heated first. The system was simulated for 10 ps at 550 K, followed by a 30 ps run at a temperature of 650 K. Next, the system was cooled stepwise. This was done in a total of 12 intermediate runs, each with a length of 10 ps, making the jumps in the temperature gradually smaller in the vicinity of the final simulation temperature of 343 K. At 343 K the liquid 18-crown-6 was simulated for a total of 30 ps. This part of the box preparation was done without a special treatment of the long-range Coulomb interactions. After the 30 ps at 343 K, the system was equilibrated for another 40 ps using the Ewald method for handling the electrostatic interactions.

All simulations were performed with a modified version of the GROMOSsimulation package[50]and used a time step of 2 fs. The liquid was simulated in the isothermal−isobaric ensemble employing a weak coupling to an external heat and pressure bath,[51] with coupling constants of respectively 0.1 and 0.5 ps^{-1}. The reference pressure was held at 1 atm. Throughout a nonbonded cutoff radius of 15 Å was used, and the covalent bonds were constrained to their equilibrium values with the SHAKE procedure.[52]

As mentioned earlier, only interactions corresponding to the nearest image convention are included in the real space sum. We used a value of $\alpha = 9.0/L$ for the convergence parameter, and 1152 vectors were included in the reciprocal space. With these settings the requirement $Q = 1$ is satisfied within 0.7×10^{-3}%. The systematic error predicted by eq 5 is found to be negligible.

3. Choice of the Force Fields

For the 18-crown-6 molecule there is unfortunately no exclusive potential available to model its intramolecular interac-

tions and its interactions with a solvent. It is for this reason that parameters have to be used which originally are devised for other classes of molecules.

In most of the published studies involving crown ethers, the AMBER all-atom force field was chosen, which was originally developed for simulations of proteins and nucleic acids.[53] In two other investigations parameters were taken from the AMBER united-atom force field in combination with Lennard-Jones parameters from Jorgensen's OPLS for proteins.[42,43] In yet a number of other studies the GROMOS force field was used, twice in combination with torsional parameters taken from the MM2 force field.[54,46] The GROMOS force field,[50] which employs the united atom approximation, was developed for molecular dynamics simulations of proteins, nucleotides, or sugars in aqueous or apolar solutions or in crystalline form.

Besides the existence of several intramolecular parameter sets that can be chosen, a number of sets of charges exist, developed for modeling the crown and its complexes with metal ions. In a previous paper a short background was given of the origin of these charges.[38] In the present study we used the following three potential models for the simulations of 18-crown-6 in the liquid state:

Potential A. The AMBER all-atom force field in combination with the charges determined by Szentpály and Shamovsky[39] ($q_O = -0.4418e$, $q_C = -0.0079e$, and $q_H = 0.1144e$). These charges resulted from a fitting procedure in which the empirical force field energies of seven conformers of the crown were fitted to their *ab initio* energies. The *ab initio* calculations included electron correlation via full second-order Møller−Plesset perturbation theory, employing the 6-31G basis set. The charges are expected to partially include the effects of intramolecular polarization. The 1−4 van der Waals interactions were scaled with a factor of 0.5. We used this force field in ref 38 and calculated a dipole moment that was in good agreement with experiment. We also stated two points of criticism concerning the above charges. With these charges, a dipole moment for dimethyl ether is found (2.14 D) which is much larger than the value reported for the gas phase (1.30 D) and which is perhaps also larger than the enhanced dipole moment expected to be found in the liquid phase. Second, there is the possibility of an overestimation of polarization effects by the way these charges were determined.

Potential B. The GROMOS united atom force field in combination with a Fourier series for the torsion potential emerging from fitting the MM2 result to the conformational space of 1,2-dimethoxyethane, without the use of nonbonded 1−4 terms.[56] The charges were taken from the electrostatic potential calculations of Singh and Kollman.[55] These calculations, for which small fragments of the crown ether were used, were done at the Hartree−Fock/6-31G* level. The charges on CH_2 and O were $0.203e$ and $-0.406e$, respectively. Apart from a slightly different charge for oxygen of $-0.4e$, this is the potential used by Kowall and Geiger in their study of the structure and dynamics of the hydration shell of 18-crown-6[54] and their calculation of the free energy for association of 18-crown-6 and K+ in water.[46] Contrary to previous investigations,[32,57] Kowall and Geiger found an activation barrier for the association process in accordance with experimental results. However, it is not entirely clear how the results of the different simulations are influenced by the simulation parameters, the employed force field, and of course the differences in the sampling techniques that were used in these studies.

Potential C. The GROMOS force field. The charges were the same as in potential B. In the GROMOS force field, the 1−4 Lennard-Jones parameters are lowered explicitly. Straatsma and McCammon[31] applied an additional scale factor of 0.5 for the Coulomb part of the 1−4 interactions.

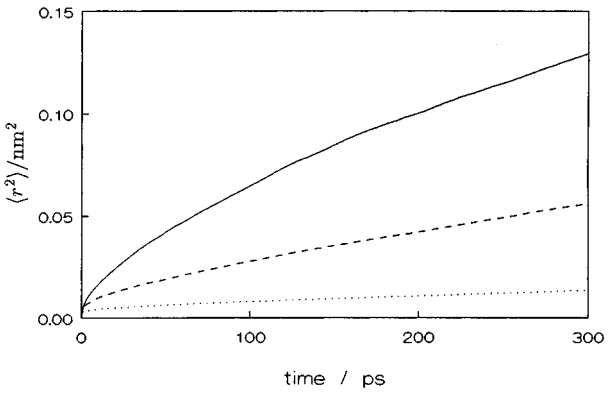

Figure 1. Mean square displacement of the center-of-masses of the molecules. The solid line corresponds with potential A, the dotted line corresponds with potential B, and the dashed line with potential C.

TABLE 1: Comparison of Some of the Properties of 18-Crown-6 for the Different Potential Models

	potential model			
	A	B	C	expt
temp/K	344	343	343	
density/g cm^{-3}	1.107	1.166	1.135	1.075[a]
$\langle \lvert \boldsymbol{\mu} \rvert \rangle$/D	3.35	4.30	2.50	3.39[a]
$\langle \mathbf{M}_x \rangle$/D	5.86	34.52	−0.22	
$\langle \mathbf{M}_y \rangle$/D	4.59	−2.05	−1.56	
$\langle \mathbf{M}_z \rangle$/D	−8.50	3.58	−0.75	
$\langle \mathbf{M}_x^2 \rangle$/D^2	542.79	1949.58	307.98	
$\langle \mathbf{M}_y^2 \rangle$/D^2	465.85	280.06	282.51	
$\langle \mathbf{M}_z^2 \rangle$/D^2	511.89	305.83	280.63	
$\langle \mathbf{M}^2 \rangle - \langle \mathbf{M} \rangle^2$/D^2	1392.9	1325.1	868.1	
ϵ	3.5	3.5	2.6	8.3[a]

[a] Reference 62.

4. Discussion

Both simulations employing the united atom approach (potential models B and C) were simulated for 1000 ps, the all-atom model (potential model A) was run for a total of 500 ps.

We have determined diffusion coefficients for the three systems from plots of the mean-square displacement vs time (Figure 1), finding $D = 2.93 \times 10^{-6}$ cm^2/s for potential A, $D = 0.28 \times 10^{-6}$ cm^2/s for potential B, and $D = 1.41 \times 10^{-6}$ cm^2/s for potential C. The results with potentials A and C are in good agreement with experimental data (1.45×10^{-6}−2.1×10^{-6} cm^2/s [58,59,60]). Together with the curves in Figure 1, this strongly suggests that the corresponding boxes are well equilibrated and not frozen. The diffusion coefficient for box B is much too small. This may indicate that the box is not well equilibrated or simply that the potential is much too flexible (see below).

4.1. Dielectric Constant. The results of the dynamics runs are presented in Table 1. It is seen that the static dielectric constants, calculated from the different simulations, are considerably smaller than the experimental value. The set of charges of potential A already takes intramolecular polarization effects into account. It is expected that inclusion of intermolecular polarization will significantly decrease the discrepancy between theory and experiment. The simulation with potential B shows a rather peculiar behavior. This behavior is discussed below.

In Figure 2, the total dipole moment fluctuation density is displayed, together with the densities of $\langle \mathbf{M}^2 \rangle$ and $\langle \mathbf{M} \rangle^2$. For

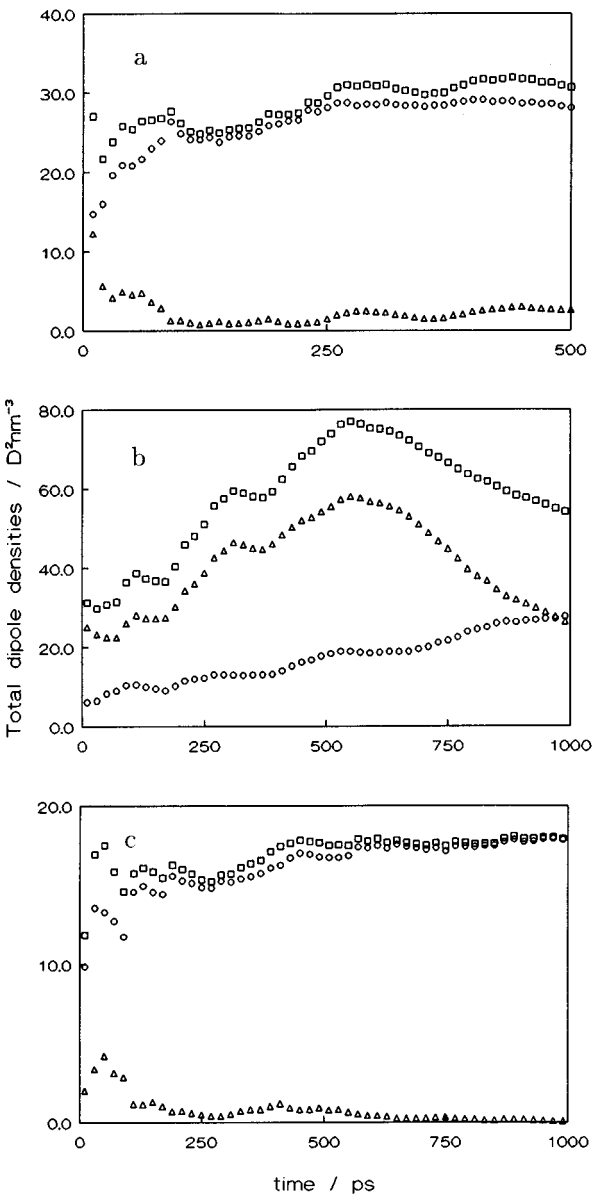

Figure 2. Running averages of the densities of the total dipole moment of the system. The squares represent $\langle M^2\rangle/V$, the triangles represent $\langle M^2\rangle/V$, and the variance $(\langle M^2\rangle - \langle M^2\rangle)/V$, is represented by the circles. (a) Results for the simulation with potential model A, (b) the simulation with potential model B, and (c) the simulation with potential model C.

potential A it seems that these densities have approximately reached equilibrium values after 500 ps. Large changes beyond 500 ps are not expected. In case of potential model C, equilibrium is reached after approximately 650 ps. For potential B, however, the fluctuation density by no means converges within 1 ns. During the first half of the run all densities continuously grow until in the second half of the run the total dipole moment collapses and the fluctuation densities start to diminish. From Table 1 we see that the *x* components of the total dipole moment is remarkably large. It was found that, by splitting up the MD run into two parts, this was entirely due to the first half of the simulation. Over the first 500 ps $\langle \mathbf{M}_x \rangle$ gave a value of 50.52 D, while the average value over the last 500 ps was not appreciably different from the average values of the other components. After approximately 500 ps drastic changes take place in the system. During the fist half of the run, relaxation processes in the fluid mainly seem to take place in two dimensions. If the crown ether molecules are pictured as a kind of disk, then reorientations apparently take place in the

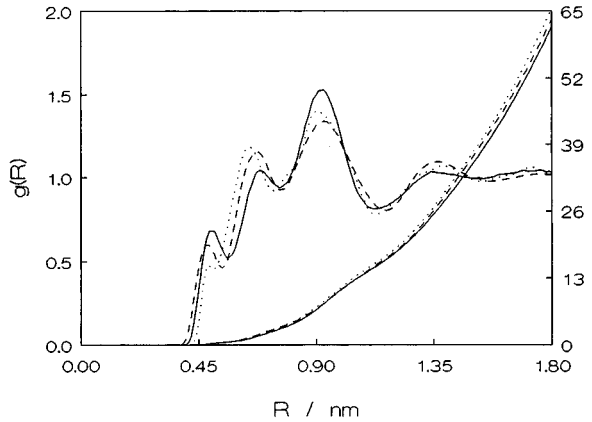

Figure 3. Radial distribution functions $g(R)$ and running coordination numbers (right *y* axis), calculated from the simulations with potential model A (solid line), with potential model B (dotted line), and with potential model C (dashed line).

plane of the molecules, and rotational motions perpendicular to the molecule's plane do not occur. If for both the first and the second 500 ps of this run the dielectric constants are calculated separately, values of respectively 2.6 and 3.2 are found. The peculiar behavior of the system with potential model B could be an indication of extreme slow fluctuations in the total dipole moment which clearly have not well been sampled. The properties of system B will be of less quality than those of the systems A and C.

In conclusion, realizing that potential models B and C only differ in the treatment of the torsional degrees of freedom, we notice that this part of the potential is of great importance for a correct description of highly flexible molecules like 18-crown-6, with many rotational isomeric states.

4.2. Liquid Structure. The large discrepancies between the calculated dielectric constants and the experimental value are most likely due to the neglect of atomic polarizabilities. The structural properties of the liquid result from the interplay between repulsive and dihedral forces, and it is to be expected that they will not be influenced by the presence or absence of atomic polarizabilities. On these grounds the examination of the liquid's structure will be valid.

In spite of the findings of the previous section we also will discuss the results with potential B because of the normal behavior observed for the mean-square displacement (Figure 1) and the fact that the results concerning the structure of the liquid are found to be virtually identical for the first and second half of that simulation (below). A comparison with the other two force fields is believed to be illustrative.

4.2.1. Spatial and Orientational Structure. We will now focus on the structure of the liquid in relation to the dielectric constant. In Figure 3, the center-of-mass radial distribution functions, $g(R)$, are given, together with the integral

$$N(R) = 4\pi\rho \int_0^R g(r) r^2 \, dr \qquad (6)$$

giving the average number of neighbor molecules (right *y* axis). ρ is the average particle number density. We discuss these distribution functions in connection with distributions, for every value of *R*, describing the relative orientations of the molecules. We have chosen to (partly) describe the orientation of the molecules by the normalized eigenvector $\boldsymbol{n}$ of the inertia tensor, belonging to the largest eigenvalue. This vector is roughly normal to the plane which minimizes the sum of the squared distances of all atoms to that plane. This makes sense since the crown ether molecules are shaped like flattened ellipsoids

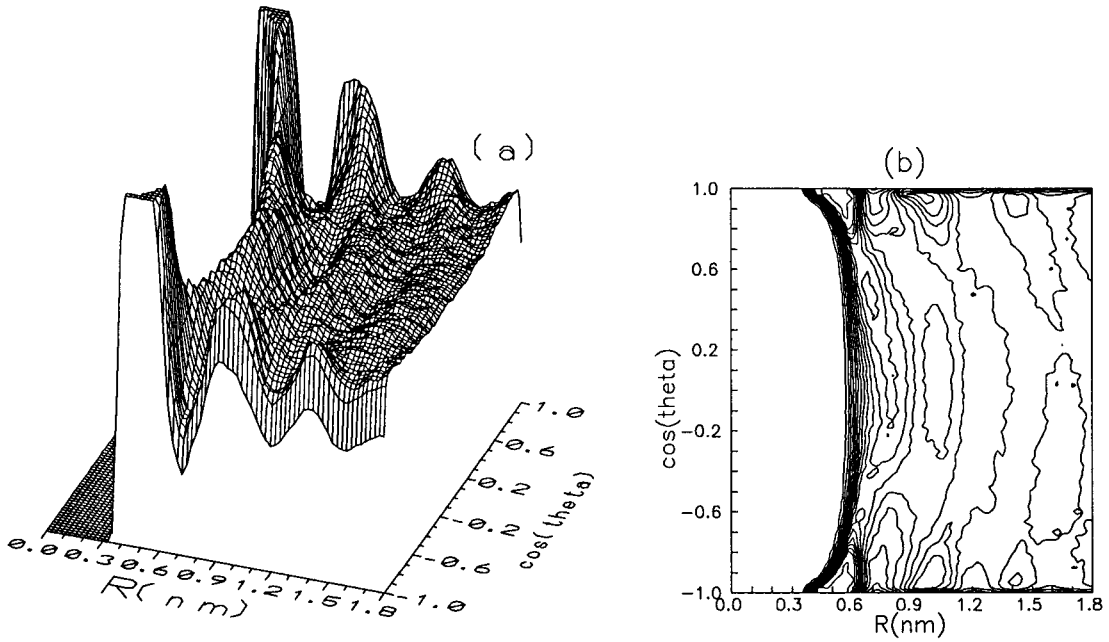

Figure 4. (a) Histograms of the cosines of the angles between the molecules as a function of the intermolecular center-of-mass separation R. The angles θ represent the angles between the eigenvectors of the inertia tensor with the largest eigenvalue (see text). The histograms are normalized for each particular value of R. Values in the z direction have been truncated. (b) Projection of (a) on lower plane. The results apply to potential A.

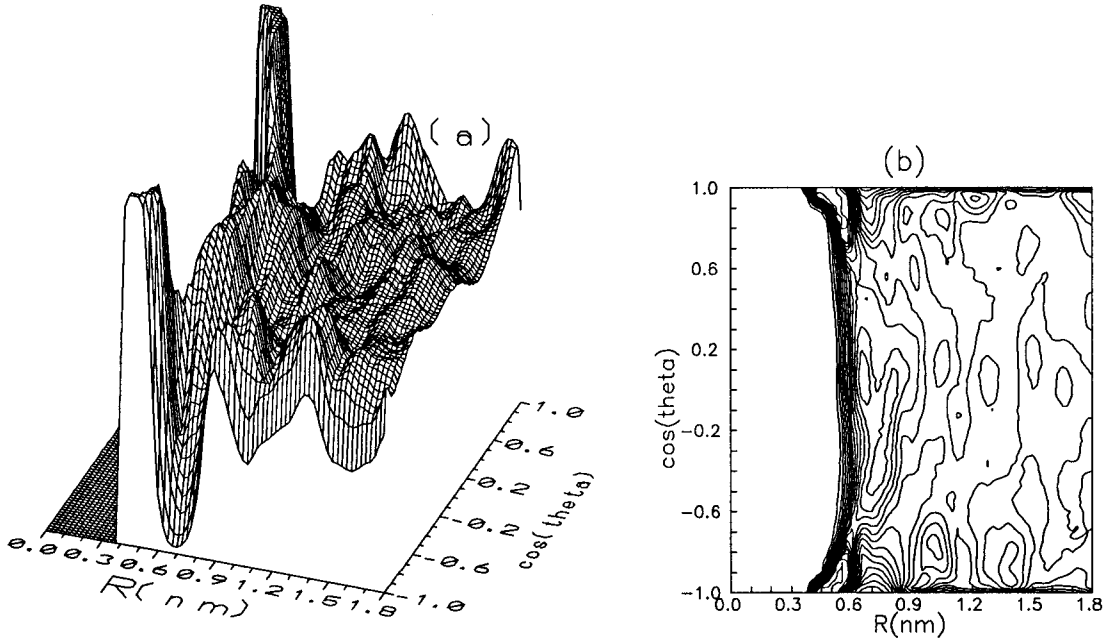

Figure 5. As Figure 4, but now for potential B.

with a rather small eccentricity in the plane of the two longest axes (see section 4.3). The relative orientation of two molecules i and j at a distance R is described by the angle $\theta_{ij}(R)$ between $\mathbf{n}_i$ and $\mathbf{n}_j$. We shall also discuss the orientational order parameter

$$S(R) = \langle 0.5(3\cos^2\theta_{ij}(R) - 1)\rangle \qquad (7)$$

The results for the three potential models are displayed in Figures 4−8.

We now first concentrate on the results obtained with potential A; these are presented in Figures 3, 4, 7, and 8. The radial distribution function, depicted in Figure 3, roughly contains three maxima and three minima. If the molecules are pictured as spheres that are only slightly penetrable, one expects a rather broad first peak starting at values of R somewhat smaller than the diameter of the spheres and extending to a first minimum around R equal to 1.5 times the sphere's diameter. The integrated number of neighbors in the first peak would then be in the order of 10. With a diameter of approximately 0.55 nm, this picture roughly applies to the radial distribution function in Figure 3. The first three maxima together then constitute the first peak. The different maxima correspond with preferred positions, which are expected to be closely related to the deviation of the molecules from being spherical.

In order to discuss this point in somewhat more detail, we present in Figure 4a, for different values of R, the distribution of the cosines of $\theta_{ij}(R)$. The graph is dominated by several peaks and ridges, which gradually disappear with increasing values of R. Since the distributions are normalized for each value of R separately, the ridges cannot be parallel to the θ axis. In order to see this more clearly, we present in Figure 4b the contour map corresponding to Figure 4a, which clearly

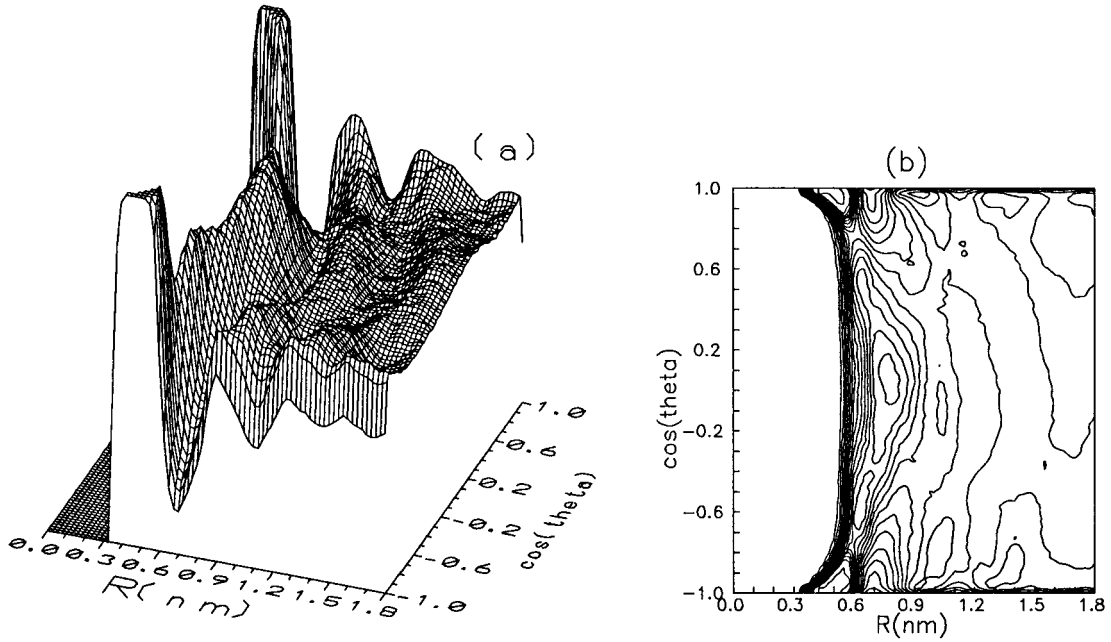

Figure 6. As Figure 4, but now for potential C.

shows the curved nature of the ridges. This property reflects the fact that for perpendicular arrangements the distance between the center-of-masses of the molecules has to be somewhat larger than for parallel packings.

Comparing Figures 3 and 4b, we see that the first two peaks and the first valley in the front plane of Figure 4a, correspond exactly with the first three maxima in Figure 3. In Figure 7 we present the distributions of $\cos\theta$ at the corresponding values of R for all three potentials. It is seen that all molecules at the smallest separations possible are almost perfectly parallel to the central molecule. The molecules in the second maximum of $g(R)$ are seen to be nonparallel, with a slight preference for the angle θ to be 60° or 120°. Then again in the next maximum, containing most of the molecules in the first coordination sphere, the molecules have a slight preference for a parallel alignment.

The order parameter $S(R)$ is given in Figure 8. In principle, it contains the same information as Figure 4. This correlation function again points out the strong correlations that exist for small intermolecular separations. The massive first peak covers distances around the first maximum in the radial distribution function. The correlation becomes negative at the second peak in $g(R)$, indicating the preference for more perpendicular arrangements at these separations. The less pronounced second peak corresponds with the third maximum in $g(R)$. At large values of R all correlations vanish, indicating that the fluid did not crystallize. (The experimental melting point of 18-crown-6 is found at 312 K.) Similar structural features as described above were found in a study on the structure of liquid benzene.[61]

We now move on to compare the results for the different potential models which are displayed in the Figures 3, 5, 6, and 8. From Figure 3 it is seen that the radial distribution functions in all three cases show roughly the same features. The places where the maxima and minima are found depend a little on the force field used. In the previous section we marked that potentials B and C only differ in the parameters for the torsional degrees of freedom. Kowall and Geiger[54] have shown that the energy barriers for some dihedral transitions are larger in the case of potential C, indicating that potential C is somewhat more rigid than potential B. Because of the larger flexibility with the latter force field entropic forces will prevent nearest neighbors to approach to very short distances, exemplified by the smaller number of particles corresponding with the first peak in the $g(R)$. On average, the molecules adopt more compact structures resulting in the second and third maximum in the distribution function to be found at smaller separations. These assumptions are supported by the somewhat larger density calculated with potential B, compared with the density obtained with potential C (see Table 1).

The differences among the force fields are better appreciated from the distributions of the cosines of $\theta_{ij}(R)$. In the case of potential B these cosines (Figure 5) are distributed much more irregularly than with potential A. The alternating preference for the parallel, the nonparallel, and again parallel alignment for values of R corresponding with the first, second, and third maximum in $g(R)$ still exists but is much less pronounced. Apparently, the molecules are packed rather disorderly. The results with potential **C** (Figure 6) compare rather well with those of potential A.

Although for potential B the function $S(R)$ (Figure 8) contains a little bit more structure, the main features are the same as for the other two potential models. Just as for potential A, the structural correlations have almost vanished at large distances for the models B and C.

4.2.2. Dipolar Structure. We now concentrate on the dipole−dipole spatial correlation function, defined as

$$\psi(R) = \langle \boldsymbol{\mu}_i \cdot \boldsymbol{\mu}_j \delta(\mathbf{r}_{ij} - \mathbf{R}) \rangle \tag{8}$$

where $\boldsymbol{\mu}_i$ and $\boldsymbol{\mu}_j$ are the dipole moment vectors of molecules i and j and r_{ij} is their separation (center-of-masses distance). In Figures 9 and 10 these functions are shown (notice the difference in the scales on the y axis).

For potential A no pronounced correlations are observed. The noisy function in Figure 9 shows only weak correlations at the values of R which correspond with the maxima in $g(R)$. Apparently, the direction of the molecular dipole moment is much more sensitive to deformations than the eigenvector of the inertia tensor. This may be understood by noticing that with this potential, which treats the hydrogen atoms explicitly, and attributes rather large charges to them, small displacements of the hydrogen atoms cause large changes in the dipole moments, while leaving the inertia tensor virtually unchanged. Also, in

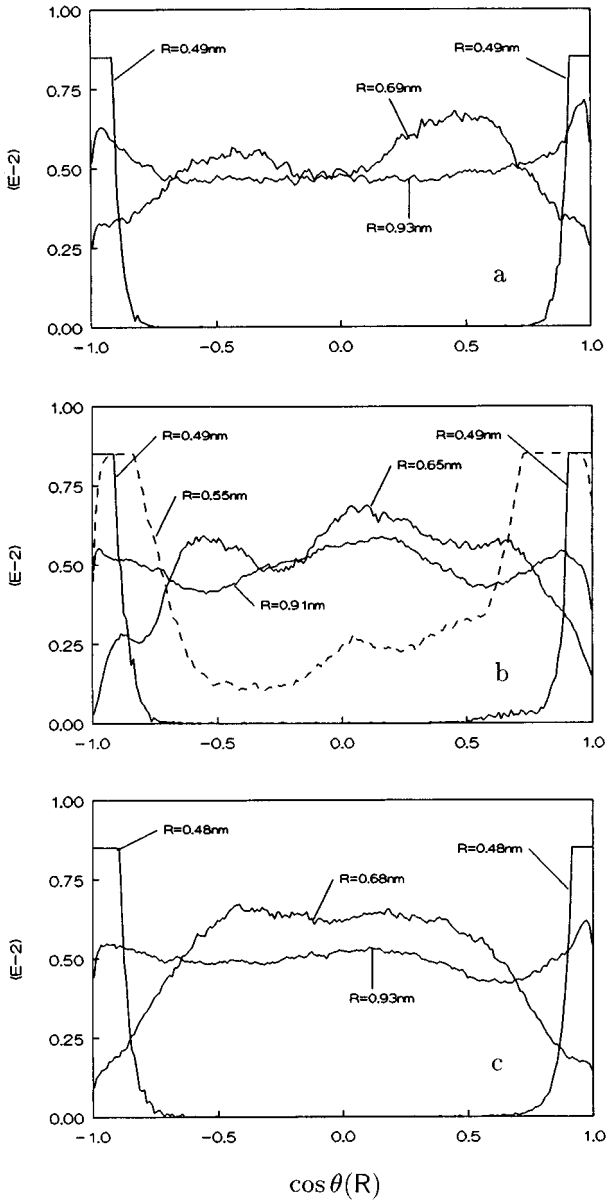

Figure 7. Distributions of $\cos\theta$ for the values of R corresponding with the maxima in the $g(R)$ (R values indicated in figure). (a) For potential A. (b) For potential B. Dashed line corresponds with R value belonging to maximum in dipole−dipole correlation function (see Figure 10 and section 4.2). (c) For potential C.

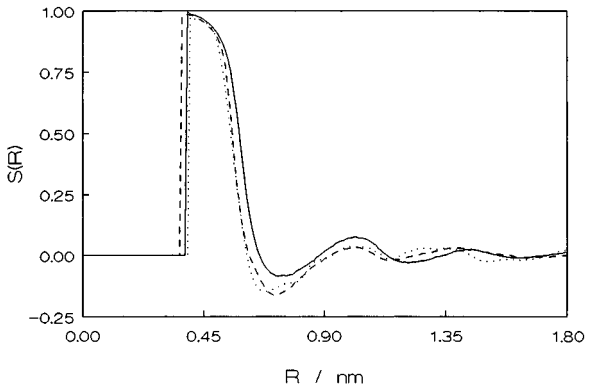

Figure 8. Orientational correlation function $S(R)$ (eq 7) for potential model A (solid line), potential model B (dotted line), and potential model C (dashed line).

the case of potential C, very weak correlations occur at those values of R which corresponding with the maxima of $g(R)$.

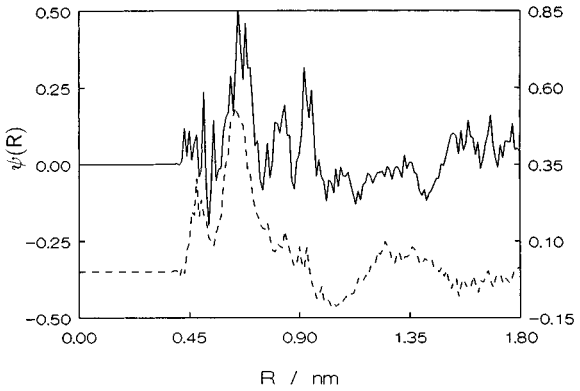

Figure 9. Dipole−dipole spatial correlation functions (eq 8). For potential model A (solid line; left y axis) and for potential model C (dashed line; right y axis).

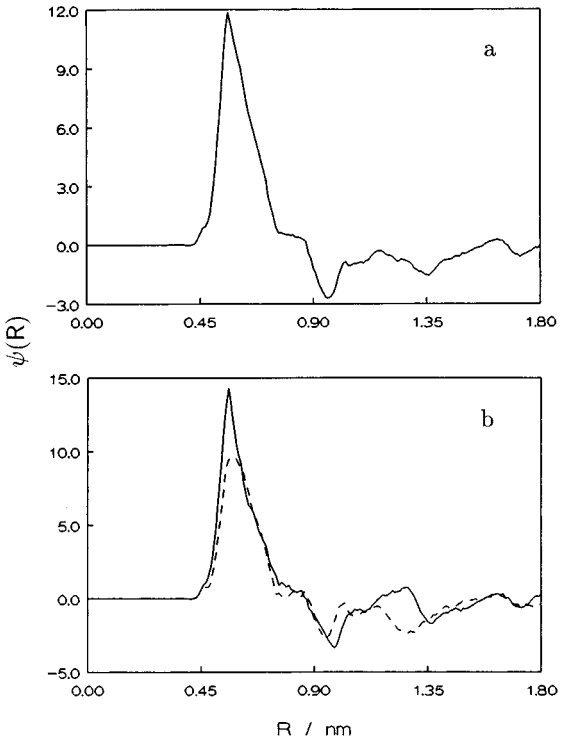

Figure 10. Dipole−dipole spatial correlation functions (eq 8) for potential B. (a) Entire MD run. (b) For the first 500 ps (solid line) and the second 500 ps of the run (dashed line).

Contrary to this behavior, very strong correlations are observed with potential B, especially at values of R near the position of the second peak of $g(R)$.

In order to understand these differences between potential B and the other two potentials somewhat better, we have made histograms of the angles between the molecular dipole moment and the different principal axes of the inertia tensor (figures not shown here). These histograms revealed a preference for the dipole moment to lie perpendicular to **n** in the case of potential A or C, and along **n** in the case of potential B. In fact, in this latter case, the dipole vector most likely makes an angle of 20°−40° with **n**.

We now first discuss the results with potential B. The dipole−dipole correlation function, $\psi(R)$, has a pronounced peak with a maximum at $R = 0.55$ nm (see Figure 10a), which is in between the position of the first and second maximum of the center-of-mass radial distribution function. In Figure 7b, we show the distribution of $\cos\theta$ at this value of R (dashed line). It is seen that almost all molecules have their axis **n** slightly tilted with respect to the **n** of the central molecule, making

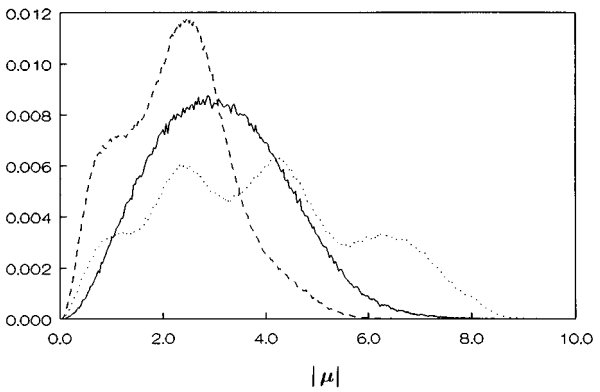

Figure 11. Distributions for the molecular dipole moments from the different molecular dynamics simulations. Solid line corresponds with potential model A, dotted line corresponds with potential model B, and dashed line corresponds with potential model C.

possible a relatively good alignment of the dipoles of the two molecules. At small values of R, $\psi(R)$ rapidly decays mainly because $g(R)$ decays. At larger values of R, the peak slowly decays until it becomes zero at $R \approx 0.85$ nm, right after the second peak in $g(R)$. Corresponding with the third peak of $g(R)$, the dipole−dipole correlation is negative.

As we have seen, with potentials A and C only very weak correlations occur. The reason for this is clear; when the molecular axes **n** are aligned, and the molecular dipoles are perpendicular to those axes, rotation around **n** destroys any dipole−dipole correlation.

To investigate the peculiar behavior of the system in the case of potential model B, observed in the previous section, we have split this simulation and examined the differences between the first and the second 500 ps. The graphs of $g(R)$ and $S(R)$ for the first and second half of the MD run were found to be approximately the same. Small differences were observed, but the discrepancies were not important. The differences between the two dipole−dipole correlation functions, which are displayed in Figure 10b, are much more outspoken. Notice that the seemingly small differences at values of R between 0.9 and 1.35 nm may be rather important since they are weighed by $4\pi R^2$ when $\langle \mathbf{M}^2 \rangle / V$ is calculated

$$\frac{\langle \mathbf{M}^2 \rangle}{V} = \frac{N}{V}\langle \mu^2 \rangle + \int_0^\infty \mathrm{d}R\, 4\pi R^2\, \psi(R) \qquad (9)$$

where $\langle \mu^2 \rangle$ is the average square molecular dipole moment. The molecular dipole moment will be examined in more detail in the following section.

4.3. The Molecular Dipole Moment. In Figure 11 histograms of the molecular dipole moments are displayed for the different simulations. For potential model A a Gaussian-like distribution is found, with an average value of 3.35 D. The same force field has been used in simulations of the crown ether *in vacuo* and in cyclohexane,[38] when the distributions showed two maxima. The averages of 3.02 and 2.94 D for respectively the vacuum simulation and the cyclohexane solution are somewhat smaller than the average found here. The distribution of conformations in the liquid phase is clearly different from that *in vacuo* and in solution. This also becomes evident if the conformations are characterized by the distribution of the atomic mass, as it was done in ref 37. By projecting the positions of the atoms onto the planes defined by the eigenvectors of the inertia tensor, density plots result as shown in Figure 12. This figure should be compared with Figure 4 from ref 38, exhibiting the densities obtained from the vacuum simulation. (In ref 37 we illustrated and discussed that dissolving 18-crown-6 in an apolar solvent hardly has any effect on the distribution of conformers.) Most striking is the strong localization of the atoms in the vacuum simulation compared with the liquid, where the atoms have a larger degree of freedom and are found to be smeared out on average. The different environment experienced by the crown ether molecules brings about a clear change in the population of conformations.

With potential B several maxima are encountered in the histogram. Also, the dipole moments are distributed over a much broader range than in the case of potentials A or C, with a significant contribution of conformations with a dipole moment between 6 and 8 D. This results in an average value of the dipole moment of 4.30 D. In the case of potential model C the distribution of small values of the dipole moment is rather similar to that of potential B, but it then rapidly goes to zero. The resulting average amounts to 2.50 D.

The histograms for the two halves of the simulation with potential B were found to be nearly identical (histograms not shown here). The averages for the molecular dipole moment are respectively 4.29 and 4.30 D for the first and second 500 ps. The changes that occurred in the system (see section 4.1) can therefore only be due to changing correlations between dipoles on different molecules, as we have seen in the previous section.

If we want to compare the molecular dipole moments obtained from the MD simulations with experimentally obtained molecular dipoles, we have to be aware of the fact that only the dielectric constant ϵ is a material property and that the fluctuations of the total dipole moment depend on the geometry and boundary conditions of the system. It seems reasonable, however, to expect that $\langle \mu^2 \rangle$ in eq 9 is much less sensitive to the precise geometry and boundary conditions than the contribution from the dipole−dipole correlations, *i.e.*, the integral over $\psi(R)$. Of course similar uncertainties exist with the experimentally determined molecular dipole moment. Usually, one uses a mean field expression to relate the experimental dielectric constant to the molecular dipole moment.

Perrin *et al.*[62] used the Onsager equation to determine the dipole moment of liquid 18-crown-6:

$$\langle \mu^2 \rangle = \frac{9kT\,\epsilon_0}{\rho}\frac{(\epsilon - \epsilon_\infty)(2\epsilon + \epsilon_\infty)}{\epsilon(\epsilon_\infty + 2)^2} \qquad (10)$$

with $\epsilon_\infty \approx n^2$, the square of the refractive index. ϵ_0 is the permittivity of the vacuum, and ρ is the number density. Equation 10 was derived for spherical particles with no specific interaction between the particles.[63] Because the 18-crown-6 molecule in the liquid state, on average, is not a spherical molecule (see Figure 12), one may think of using the Onsager equation for ellipsoidal particles[63] to calculate the molecular dipole moment:

$$\langle \mu^2 \rangle = \frac{3kT\,\epsilon_0}{\rho}\frac{(\epsilon - \epsilon_\infty)(2\epsilon + 1)}{\epsilon(2\epsilon + \epsilon_\infty)}\frac{\{\epsilon + (\epsilon_\infty - \epsilon)A_\alpha\}^2}{\{\epsilon + (1-\epsilon)A_\alpha\}\{1 + (\epsilon_\infty - 1)A_\alpha\}^2} \qquad (11)$$

where

$$A_\alpha = \frac{abc}{2}\int_0^\infty \frac{\mathrm{d}s}{(s+\alpha^2)[(s+a^2)(s+b^2)(s+c^2)]^{1/2}} \qquad (12)$$

and a, b, and c are the lengths of the semiaxes of the ellipsoid. α is equal to the length of the semiaxis along which $\boldsymbol{\mu}$ has its

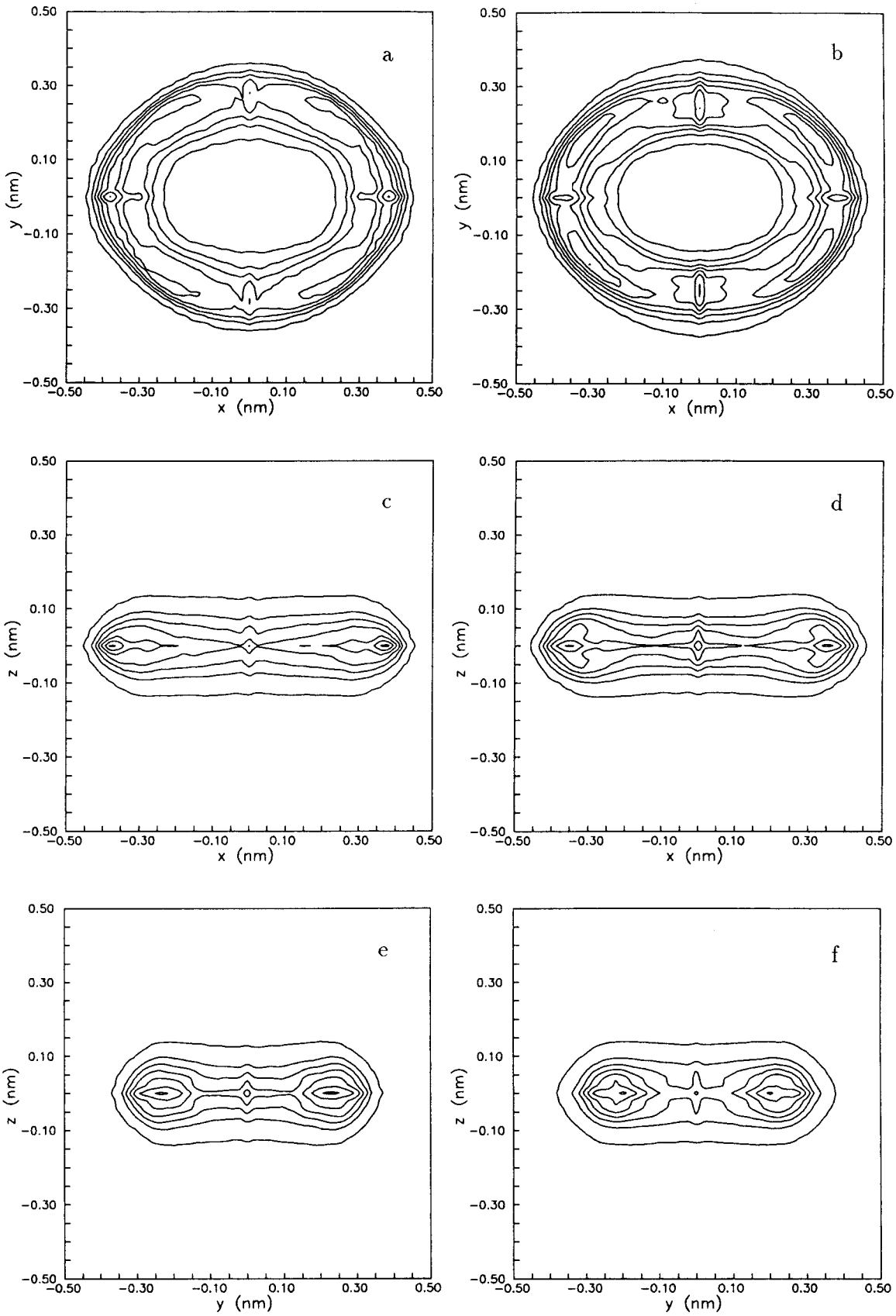

Figure 12. Contour plots from the simulation with potential model A: (a) projection of the positions of the oxygen atoms of the crown ether on the *xy* plane; (b) projection of the carbon atoms on the *xy* plane; (c) projection of the oxygen atoms on the *xz* plane; (d) projection of the carbon atoms on the *xz* plane; (e) projection of the oxygen atoms on the *yz* plane; (f) projection of the carbon atoms on the *yz* plane. (Compare with Figure 4 from ref 38.) The *z* axis is formed by the eigenvector belonging to the largest eigenvalue of the inertia tensor (the vector **n** in section 4.2). The *x* and *y* axes lie in the plane of the molecule and are perpendicular to the *z* axis. The *x* axis corresponds with the smallest eigenvalue.

largest component. Since *a*, *b*, and *c* may be calculated from the simulation data, we have available all data to calculate semiexperimental molecular multipoles from eq 11. In case of a sphere, A_α takes the value of $^1/_3$ and eq 11 reduces to eq 10.

TABLE 2: Root-Mean-Square Molecular Dipole Moments Calculated for the Different Dynamics Simulations; Minimum and Maximum Values Found Are Also Given

force field	av value[a]/D	min value/D	max value/D
A	3.347 (1.290)	0.031	9.242
B	4.296 (1.916)	0.013	9.664
C	2.501 (1.059)	0.014	7.675

[a] Standard deviations are given in parentheses. Experimentally, a dipole moment of 3.39 D was found for 18-crown-6 in the liquid phase at 343 K (ref 62).

TABLE 3: Molecular Dipole Moments Calculated from Eqs 10 and 11, Using Both the Experimental Value for ϵ and the ϵ Computed from the Simulation

force field	depolarization factor A_a, A_b, A_c	μ_{ell}/D ($\exp \epsilon$)	μ_{ell}/D (ϵ MD run)	μ_{ons}/D ($\exp \epsilon$)	μ_{ons}/D (ϵ MD run)
A	0.1702	4.13	1.99	3.39	1.73
	0.2254[a]	3.86	1.89		
	0.6036	2.50	1.44		
B	0.1393	4.30	2.05	3.39	1.61
	0.1893	4.04	1.96		
	0.6586[a]	2.35	1.40		
C	0.1040	4.50	1.27	3.39	0.96
	0.1531[a]	4.23	1.22		
	0.7014	2.25	0.90		

[a] Depolarization factor belonging to the semiaxis along which the dipole moment prefers to align.

From eq 12 it is seen that only relative measures are needed for the semiaxis a, b, and c. We have chosen to diagonalize the "inertia tensor" with all masses equal to one and to define $a \sim (\sum_i x_i^2)^{1/2}$, with x_i the component of atom i along the eigenvector of the smallest "moment of inertia". Similar definitions hold for b and c, with increasing values of the "moments of inertia".

The results obtained from eqs 10 and 11, for both the experimental and the computed dielectric constant, are given in Table 3. For potentials A and C, for which the depolarization factor is associated with an axis in the plane of the molecule, the dipole moments emerging from eq 11, using the experimental dielectric constant, are substantially larger than the value reported by Perrin *et al.* and also larger than those calculated from the simulations. In the case of potential B, when the depolarization factor is found to be perpendicular to the plane of the molecule, the predicted dipole moment is much smaller than the one reported by Perrin *et al*. or the value calculated from the MD run. Together with the results obtained with this force field in previous sections, it is considered not to give a satisfying description of liquid 18-crown-6. Potential models A and C seem more reliable.

Comparing the results of eq 10 and eq 11 using the dielectric constant from the simulations shows that the results are a little bit better if the shape of the molecules is taken into account.

Although there is a rather good agreement between the experimental and theoretical molecular dipole moments, especially for potential A, this must be accidental. Despite this perfect agreement there is a large difference between the experimental and calculated dielectric constant.

5. Conclusions

We have performed molecular dynamics simulations of liquid 18-crown-6 using three different potential models. Characteristic of potential A is that it explicitly treats the hydrogen atoms; it also implicitly takes intramolecular polarization effects into account. Characteristic of potential B is that it has low barriers for dihedral transitions and is therefore rather flexible. Potential C is the one standardly used with the GROMOS package.

The center-of-mass radial distribution functions predicted with all three models were roughly the same. Also, the correlations between molecular separations and mutual orientations were very similar in all three cases. At the shortest intermolecular separations the molecules are oriented parallel. At distances corresponding to the second maximum in $g(R)$ the molecules prefer nonparallel orientations. Around the third peak in $g(R)$, there is again a slight preference for parallel orientations. We believe that these characteristics are roughly in accordance with the behavior of real 18-crown-6. Only with potential B, the flexible potential, were these correlations less pronounced at the larger values of R.

We have used structural information from the molecular dynamics simulations to obtain semiexperimental molecular dipole moments from the experimental dielectric constant, using the Onsager expression for elliptical molecules. In the the case of potential models A and C, the nonspherical symmetry had only moderate effect on the molecular dipole moment. In the case of potential B the influence was more substantial, lowering the dipole moment by approximately 25%. The theoretical dipole moment with potential A is close to the experimental one. This agreement must be met with some skepticism in view of the approximate nature of the Onsager equation.

The dielectric constants predicted with all three models disagree very much with the experimental one. Since this is the only hard comparison made, all three potentials must be considered unsatisfactory. We believe that explicitly adding electronic polarization terms to the potential will greatly ameliorate the situation. One of the things which may happen in that case, is a much larger contribution from the integral in eq 9, without necessarily a large influence on the structural properties of the liquid. Second, we think that explicitly treating the hydrogen atoms also contributes to the possibility of large dipole fluctuations and thus to a larger dielectric constant. Finally, we think that potential B is much too flexible.

References and Notes

(1) Adams, D. J. *Mol. Phys.* **1980**, *40*, 1261.
(2) Adams, D. J.; Adams, E. M. *Mol. Phys.* **1981**, *42*, 907.
(3) Neumann, M.; Steinhauser O. *Chem. Phys. Lett.* **1983**, *95*, 417.
(4) Onsager, L. *J. Am. Chem. Soc.* **1936**, *58*, 1486.
(5) Kirkwood, J. G. *J. Chem. Phys.* **1939**, *7*, 911.
(6) Barker, J. A., and Watts, R. O. *Mol. Phys.* **1973**, *26*, 789.
(7) Ewald, P. *Ann. Phys.* **1921**, *64*, 253.
(8) de Leeuw, S. W.; Perram J. W.; Smith, E. R. *Proc. R. Soc. London, Ser. A* **1980**, *373*, 27.
(9) Neumann, M.; Steinhauser, O. *Mol. Phys.* **1980**, *39*, 437.
(10) Neumann, M. *Mol. Phys.* **1983**, *50*, 841.
(11) Neumann, M.; Steinhauser, O. *Chem. Phys. Lett.* **1983**, *102*, 508.
(12) Neumann, M.; Steinhauser, O.; Pawley, G. S. *Mol. Phys.* **1984**, *52*, 97.
(13) Neumann, M.; Steinhauser, O. *Chem. Phys. Lett.* **1984**, *106*, 563.
(14) Neumann, M. *Mol. Phys.* **1986**, *57*, 97.
(15) Neumann, M. *Mol. Phys.* **1986**, *60*, 225.
(16) Petersen, H. G.; de Leeuw, S. W.; Perram, J. W. *Mol. Phys.* **1989**, *66*, 637.
(17) Kusalik, P. G. *Mol. Phys.* **1989**, *67*, 67.
(18) Kusalik, P. G.; Mandy, M. E.; Svishchev, I. M. *J. Chem. Phys.* **1994**, *100*, 7654.
(19) Neumann, M. *J. Chem. Phys.* **1986**, *85*, 1567.
(20) Anderson, J.; Ullo, J. J.; Yip, S. *J. Chem. Phys.* **1987**, *87*, 1726.
(21) Alper, H. E.; Levy, R. M. *J. Chem. Phys.* **1989**, *91*, 1242.
(22) Reddy, M. R.; Berkowitz, M. *Chem. Phys. Lett.* **1989**, *155*, 173.
(23) Belhadj, M.; Alper, H. E.; Levy, R. M. *Chem. Phys. Lett.* **1991**, *179*, 13.
(24) Smith, P. E.; van Gunsteren, W. F. *J. Chem. Phys.* **1994**, *100*, 3169.
(25) Smith, P. E.; Brunne, R. M.; Mark, A. E.; van Gunsteren, W. F. *J. Phys. Chem.* **1993**, *97*, 2009.
(26) Bovill, M. J.; Chadwick, D. J.; Sutherland, I. O. *J. Chem. Soc., Perkin Trans.* **1980**, *2*, 1529.
(27) Wipff, G.; Weiner, P. K.; Kollman, P. A. *J. Am. Chem. Soc.* **1982**, *104*, 3249.

(28) Weiner, P. K.; Profeta, S., Jr.; Wipff, G.; Havel, T.; Kuntz, I. D.; Langridge, R.; Kollman, P. A. *Tetrahedron* **1983**, *39*, 1113.
(29) Howard, A. E.; Singh, U. C.; Billeter, M.; Kollman, P. A. *J. Am. Chem. Soc.* **1988**, *110*, 6984.
(30) Billeter, M.; Howard, A. E.; Kuntz. I. D.; Kollman, P. A. *J. Am. Chem. Soc.* **1988**, *110*, 8385.
(31) Straatsma, T. P.; McCammon, J. A. *J. Chem. Phys.* **1989**, *91*, 3631.
(32) Dang, L. X.; Kollman, P. A. *J. Am. Chem. Soc.* **1990**, *112*, 5716.
(33) Ha, Y. L.; Chakraborty, A. K. *J. Phys. Chem.* **1991**, *95*, 10781.
(34) Sun, Y.; Kollman, P. A. *J. Comput. Chem.* **1992**, *13*, 33.
(35) Leuwerink, F. T. H.; Harkema, S.; Briels, W. J.; Feil, D. *J. Comput. Chem.* **1993**, *14*, 899.
(36) Troxler, L.; Wipff, G. *J. Am. Chem. Soc.* **1994**, *116*, 1468.
(37) Leuwerink, F. T. H.; Briels, W. J. *J. Chem. Phys.* **1995**, *103*, 4637.
(38) Leuwerink, F. T. H.; Briels, W. J. *J. Phys. Chem.* **1995**, *99*, 16549.
(39) von Szentpály, L.; Shamovsky, I. L. *J. Mol. Struct. (THEOCHEM)* **1994**, *305*, 249.
(40) van Eerden, J.; Harkema, S.; Feil, D. *Acta Crystallor.* **1990**, *B46*, 222.
(41) van Eerden, J.; Harkema, S.; Feil, D. *J. Phys. Chem.* **1988**, *92*, 5076.
(42) Mazor, M. H.; McCammon, J. A.; Lybrand, T. P. *J. Am. Chem. Soc.* **1989**, *111*, 55.
(43) Mazor, M. H.; McCammon, J. A.; Lybrand, T. P. *J. Am. Chem. Soc.* **1990**, *112*, 4411.
(44) Dang, L. X.; Kollman, P. A. *J. Phys. Chem.* **1995**, *99*, 55.
(45) Sun, Y.; Kollman, P. A. *J. Am. Chem. Soc.* **1995**, *117*, 3599.
(46) Kowall, T.; Geiger, A. *J. Phys. Chem.* **1995**, *99*, 5240.
(47) Allen, M. P.; Tildesley, D. J. 1987 *Computer Simulation of Liquids*; Clarendon: Oxford.
(48) Heyes, D. M. *CCP5 Q.* **1983**, *8*, 29.
(49) Kusalik, P. G. *J. Chem. Phys.* **1990**, *93*, 3520.
(50) van Gunsteren, W. F.; Berendsen, H. J. C. Groningen Molecular Simulation Library, Groningen, The Netherlands, 1987.
(51) Berendsen, H. J. C.; Postma, J. P. M.; van Gunsteren, W. F.; DiNola, A.; Haak, J. R. *J. Chem. Phys.* **1984**, *81*, 3684.
(52) Ryckaert, J.; Ciccoti, G.; Berendsen, H. J. C. *J. Comput. Phys.* **1977**, *23*, 327.
(53) Weiner, S. J.; Kolmann, P. A.; Nguyen, D. T.; Case, D. A. *J. Comput. Chem.* **1986**, *7*, 230.
(54) Kowall, T.; Geiger, A. *J. Phys. Chem.* **1994**, *98*, 6216.
(55) Singh, U. C.; Kollman, P. A. *J. Comput. Chem.* **1984**, *5*, 129.
(56) Bressanini, D.; Gamba, A.; Morosi, G. *J. Phys. Chem.* **1990**, *94*, 4299.
(57) van Eerden, J.; Briels, W. J.; Harkema, S.; Feil, D. *Chem. Phys. Lett.* **1989**, *164*, 370.
(58) Vogel, H.; Weiss, A. *Ber. Bunsen-Ges. Phys. Chem.* **1980**, *85*, 539.
(59) Lassegues, J. C.; Fouassier, M.; Viovy, J. L. *Mol. Phys.* **1983**, *50*, 417.
(60) Richter, H.; Zeidler, M. D. *Mol. Phys.* **1985**, *55*, 49.
(61) Evans, D. J.; Watts, R. O. *Mol. Phys.* **1976**, *32*, 93.
(62) Perrin, R.; Decoret, C.; Bertholon, G.; Lamartine, R. *Nouv. J. Chim.* **1983**, *7*, 263.
(63) Böttcher, C. J. F.; van Belle, O. C.; Bordewijk, P.; Rip, A. *Theory of Electric Polarization*; Elsevier: Amsterdam, 1973; Vol. 1.